materials

MDPI

Article

Enhanced Thermoelectric Performance of Cu_2SnSe_3-Based Composites Incorporated with Nano-Fullerene

Degang Zhao *, Jiai Ning, Di Wu and Min Zuo

School of Materials Science and Engineering, University of Jinan, 336 Nan-Xinzhuang West Road, Jinan 250022, China; crystal4885@sina.com (J.N.); 18366100143@163.com (D.W); mse_zuom@ujn.edu.cn (M.Z.)
* Correspondence: mse_zhaodg@ujn.edu.cn; Tel.: +86-531-8276-7561

Academic Editor: Shankar M.L. Sastry
Received: 29 June 2016; Accepted: 21 July 2016; Published: 28 July 2016

Abstract: In this study, nano-sized fullerene C_{60} powder was sufficiently mixed with Cu_2SnSe_3 powder by ball milling method, and the C_{60}/Cu_2SnSe_3 composites were prepared by spark plasma sintering technology. The fullerene C_{60} distributed uniformly in the form of clusters, and the average cluster size was less than 1 μm. With increasing C_{60} content, the electrical conductivity of C_{60}/Cu_2SnSe_3 composites decreased, while the Seebeck coefficient was enhanced. The thermal conductivity of composites decreased significantly, which resulted from the phonon scattering by the C_{60} clusters located on the grain boundaries of the Cu_2SnSe_3 matrix. The highest figure of merit ZT of 0.38 was achieved at 700 K for 0.8% C_{60}/Cu_2SnSe_3 composite.

Keywords: thermoelectric alloy; composites; Cu_2SnSe_3; C_{60}

1. Introduction

Thermoelectric (TE) materials have attracted increasing worldwide attention due to their potential application in electronic cooling, waste heat recovery, and power generation [1–4]. The conversion efficiency of TE materials is determined by the dimensionless figure of merit, $ZT = \alpha^2\sigma T/\kappa$, where α is the Seebeck coefficient, σ is the electrical conductivity, T is the absolute temperature, and κ is the total thermal conductivity. The total thermal conductivity is composed of an electron part (κ_E) and a phonon part (κ_L). Therefore, to maximize the ZT value of TE materials, a large α and σ, as well as a low κ are required. In recent years, several classes of bulk materials with high ZT have been discovered and developed, such as skutterudites, clathrates, and Cu-based chalcogenide semiconductors.

Cu-based chalcogenide compounds with a diamond-like structure, such as ternary Cu_2MSe_3 (M = Sn, Ge) and Cu_3SbSe_4, have attracted a lot of attention recently, due to their quite low thermal conductivity. In several Cu-based chalcogenide compound systems, the Cu_2SnSe_3 structure has partial "phonon glass electron crystal" (PGEC) characteristic, which makes it possible to achieve high TE performance. The Cu-Se bond network dominates the electron conduction, while the contribution from the element Sn is very weak; thus, the Sn site is suitable for optimization of the TE property. Various attempts, including doping by partial substitution, have been made to improve the thermoelectric properties of Cu_2SnSe_3 compound [5–7]. Shi et al. have reported the In-doped $Cu_2In_xSn_{1-x}Se_3$ and the maximum ZT value reaches 1.14 at 850 K for $Cu_2In_{0.1}Sn_{0.9}Se_3$ sample [8]. Fan et al. fabricated the $Cu_2Ga_xSn_{1-x}Se_3$ samples using hot-press sintering technique and achieved the ZT value of 0.43 for $Cu_2Ga_{0.075}Sn_{0.925}Se_3$ sample [9]. In addition, Skoug, et al. also confirmed that doping with isoelectronic Ge on the Sn site is also effective in enhancing the ZT value [10]. Aside from doping, the dispersion of nanostructure phases into the thermoelectric matrix is also an attractive approach to improving the performance of TE materials. However, the Cu_2SnSe_3-based thermoelectric composites are scarcely

investigated, because the enhancement of ZT is unapparent compared with the doping. Although significant reduction in the lattice conductivity can be achieved via enhanced phonon scattering at grain boundaries or matrix/inclusion interfaces, the electrical conductivity of TE composites also decreases, resulting in a marginal improvement of the overall ZT value. In addition, good selection of the dispersed phase and the control of microstructure are also required for TE composite [11–14]. Therefore, effective enhancement of ZT for TE composites depends on the microstructure of composites—i.e., the distribution or the shape of the component.

Fullerene C_{60} has very high elastic modulus and is a chemically-stable nonpolar fullerene molecule. C_{60} and C_{60}-decorated grain boundaries may provide an effective phonon scattering, which could decrease the lattice thermal conductivity. Meanwhile, the scattering of charge carriers (electrons or holes) by the C_{60} could be ineffective due to the large value of electron (hole) wavelength compared to a fullerene molecule size. Blank and Kulbachinskii, et al. reported that the addition of 0.5 vol % C_{60} improved the TE properties of $Bi_{0.5}Sb_{1.5}Te_3$ material, and the ZT value obtained was 1.17 at 450 K [15,16]. Shi, et al. found that adding 6.5 mass% C_{60} into pure $CoSb_3$ can increase the ZT value, while adding amounts between 0.5% and 4.8% into $CoSb_3$ decreased the ZT value [17]. The similar results of Itoh, et al. showed that the maximum ZT value for the 1% $C_{60}/Co_{0.92}Ni_{0.08}Sb_{2.96}Te_{0.04}$ composite was 0.62 at 800 K, which was evidently higher than that of C_{60}-free sample [18]. Nandihalli, et al. also reported that the ZT value of $C_{60}/Ni_{0.05}Mo_3Sb_{5.4}Te_{1.6}$ composites was enhanced in the whole temperature range due to the large decrease of κ_L [19]. In this contribution, we attempted to introduce the C_{60} into a Cu_2SnSe_3 system and expected to achieve a larger reduction in the thermal conductivity of C_{60}/Cu_2SnSe_3 composites.

In the present work, the fullerene C_{60} powder was incorporated into Cu_2SnSe_3 matrix using ball milling (BM), and C_{60}/Cu_2SnSe_3 composites were fabricated by spark plasma sintering (SPS) technology. Effects of C_{60} particles on the thermoelectric properties of C_{60}/Cu_2SnSe_3 composites were discussed, and the results are beneficial to the development of Cu_2SnSe_3-based composites with high performance using BM-SPS technology.

2. Experimental Procedures

The polycrystalline Cu_2SnSe_3 samples were synthesized by melting method. The stoichiometric amount of starting materials Cu (powder, 99.95%), Sn (powder, 99.999%), and Se (shot, 99.999%) were first placed in a carbon crucible enclosed in evacuated fused-silica ampoules. The ampoules were slowly heated to 1173 K and held for 12 h in a vertical furnace. Then, the ampoules were slowly cooled to 873 K in 24 h, followed by annealing at this temperature for 2 days. Finally, the obtained ingots were ground into fine powder. Commercially available fullerene powder with average particle size of 500 nm (XFNANO, Nanjing, China) was chosen as the nanoinclusion, as shown in Figure 1. The fullerene C_{60} purity is 99.98%, and the other 0.02% refers to impurities of C_{70} and other carbon structures. The fullerene C_{60} powder was added into the Cu_2SnSe_3 powder at fractions of 0.4, 0.8, 1.2, and 1.6 vol %, respectively. Then, the C_{60}-added Cu_2SnSe_3 powders were mechanically ground with planetary ball milling equipment at 150 rpm for 240 min. The as-milled powders were sintered by spark plasma sintering (SPS 2040) at around 860 K for about 8 min under uniaxial pressure of 50 MPa in vacuum.

The density of the sintered C_{60}/Cu_2SnSe_3 composites was measured using the Archimedes method. The constituent phases of the samples were determined by X-ray diffractometry (Cu K_α, Rigaku, Rint2000, Tokyo, Japan). The chemical composition of bulk samples was characterized using electron probe micro-analysis (EPMA, JEOL, JXA-8100, Tokyo, Japan) with a wavelength dispersive spectrometer (WDS). The composition was calculated by averaging five spots. The microstructure of all C_{60}/Cu_2SnSe_3 composites was observed by high-resolution transmission electron microscopy (HRTEM, JEM2100F, JEOL, Tokyo, Japan). The thermal diffusivity (λ) was measured by laser flash method (Netzsch LFA427) in a flowing Ar atmosphere between 300 and 700 K. The thermal conductivity was calculated from the relationship $\kappa = \rho\lambda C_p$, where ρ is the density of the sintered sample and

C_p is the specific heat capacity. The electrical conductivity and Seebeck coefficient were measured simultaneously using commercial equipment (ZEM-3, ULVAC-RIKO, Tokyo, Japan) on a bar-type sample with a dimension of 2 × 2 × 10 mm^3. The Hall coefficient (R_H) was measured using the van der Pauw's method in vacuum with a magnetic field of 2 T. The carrier concentration (p_H) and mobility (μ_H) were estimated from the relations of $p_H = 1/(eR_H)$ and $\mu_H = \sigma R_H$, based on the assumption of single band model, where e is the electronic charge. All measurements were performed in a temperature range of 300–700 K.

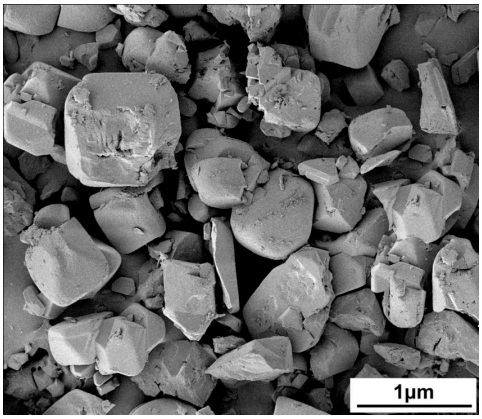

Figure 1. SEM image of fullerene powder with average particle size of 500 nm.

3. Results and Discussion

3.1. Microstructure and XRD Analysis

Figure 2 shows the SEM image of the 1.6 vol % C_{60}-added Cu_2SnSe_3 powder after ball milling. It can be observed that the average particle size of milled C_{60}/Cu_2SnSe_3 powder was about 100 nm. Figure 3 shows the X-ray diffraction patterns of xC_{60}/Cu_2SnSe_3 composites (x = 0, 0.4, 0.8, 1.2, and 1.6 vol %) after SPS. The measured relative densities for all C_{60}/Cu_2SnSe_3 composites after SPS are above 97% of the theoretical value. The diffraction peaks in Figure 3 are well-indexed based on the JCPDS 65-4145 (Joint Committee on Powder Diffraction Standards) of Cu_2SnSe_3. As the content of C_{60} in the composites is very low, the diffraction peak of C_{60} is not found in the XRD pattern of all C_{60}/Cu_2SnSe_3 samples. Therefore, all C_{60}/Cu_2SnSe_3 samples show the same XRD patterns with the pure Cu_2SnSe_3 sample.

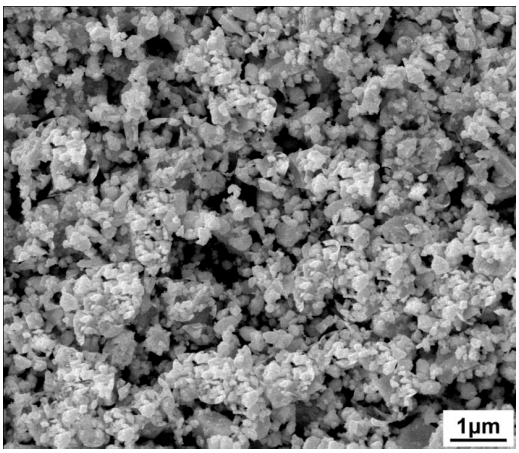

Figure 2. SEM image of the 1.6 vol % C_{60}/Cu_2SnSe_3 powder after ball milling.

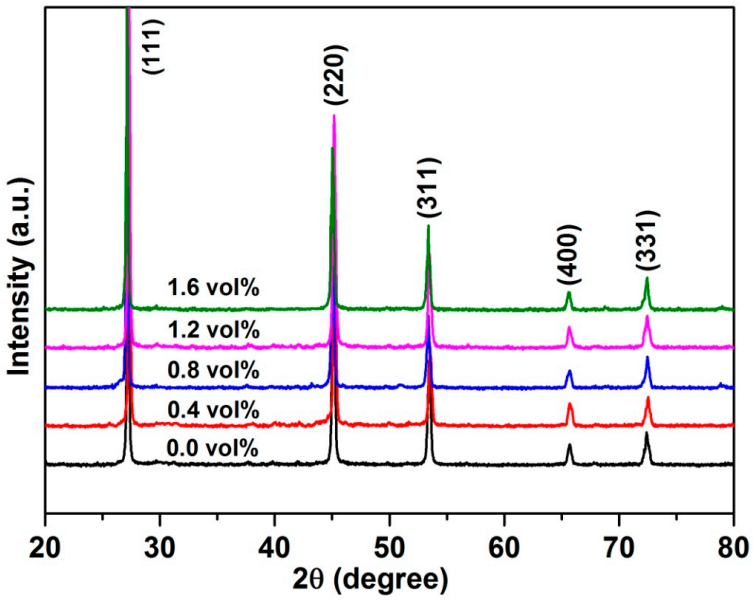

Figure 3. XRD patterns of sintered C_{60}/Cu_2SnSe_3 composites.

Figure 4a,b show the SEM microstructure of the sintered pure Cu_2SnSe_3 sample and 1.6 vol % C_{60}/Cu_2SnSe_3 composite, respectively. The fullerene C_{60} distributed uniformly in the form of clusters, and the average cluster size was lower than 1 μm. Shi, et al. reported that in the $CoSb_3$ material, most of the C_{60} molecules agglomerate into irregular micrometer-size clusters located at the grain boundaries [17]. The smaller size of clusters in this study should be due to the ball milling technology. The chemical composition of C_{60}/Cu_2SnSe_3 composites was characterized by SEM and energy-dispersive X-ray spectroscopy (EDS), as shown in Figure 5. The results of EDS also confirm that the matrix was analyzed to be composed of 33.53 at. %; Cu, 16.85 at. %; Sn, and 49.62 at. %; Se, corresponding to the Cu_2SnSe_3 phase. The black phase only contains C element, indicating C_{60} phase. To further analyze the C_{60} clusters in the C_{60}/Cu_2SnSe_3 composite, HRTEM of C_{60}/Cu_2SnSe_3 composite was carried out, as shown in Figure 6. The size of C_{60} is about 80 nm, which means the ball milling process decreases the average size of C_{60} particles. According to the theory proposed by Faleev and Zebardaji, et al. [20,21], nano-phases that distribute in the thermoelectric matrix can result in strain fields, which could cause some changes in the band structure of the material and then greatly influence its thermoelectric properties.

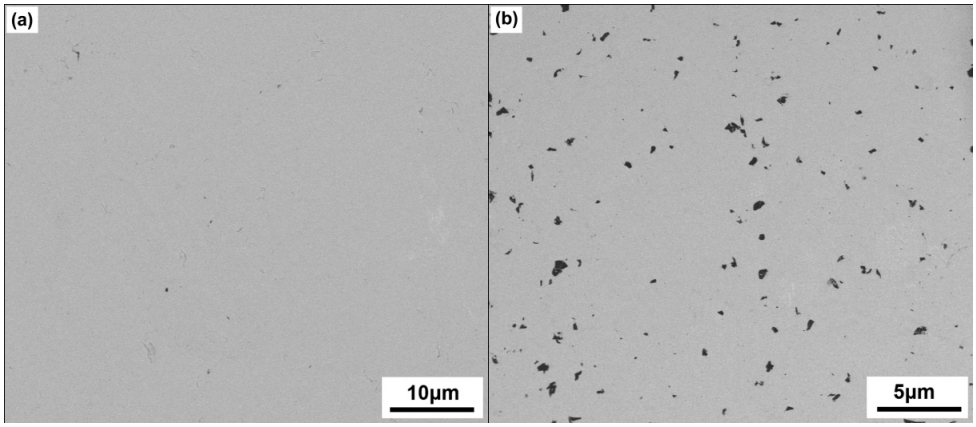

Figure 4. (**a**) SEM microstructure of the sintered pure Cu_2SnSe_3; (**b**) SEM microstructure of sintered 1.6 vol % C_{60}/Cu_2SnSe_3 composite.

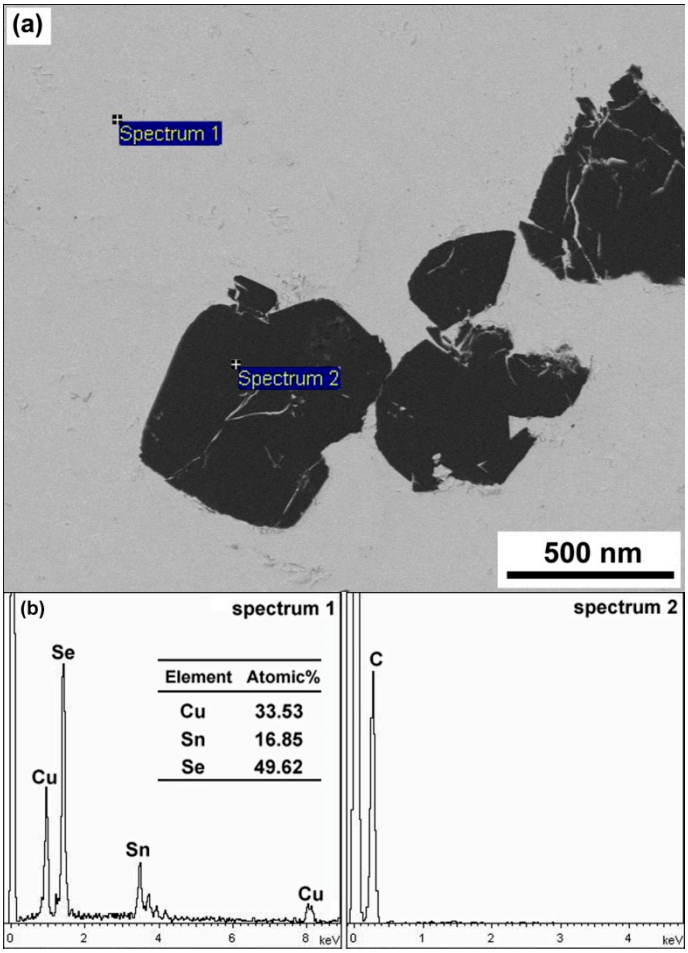

Figure 5. (**a**) SEM image of the sintered 1.6% C_{60}/Cu_2SnSe_3 composite; (**b**) energy-dispersive X-ray spectroscopy (EDS) results of Cu_2SnSe_3 matrix and C_{60} phase.

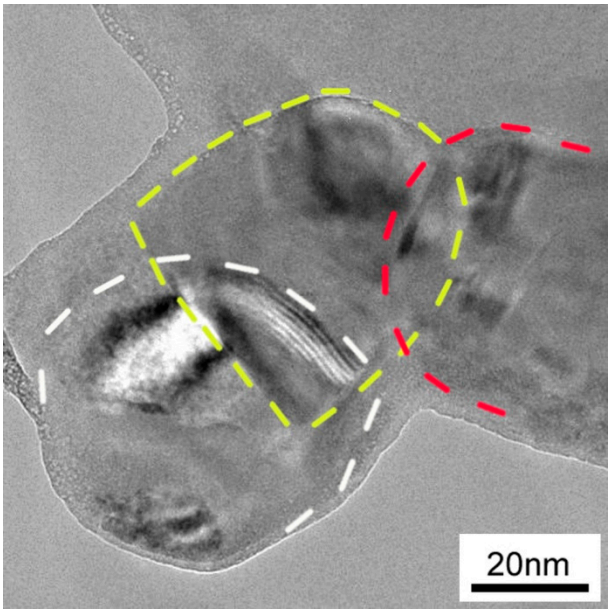

Figure 6. High-resolution transmission electron microscopy (HRTEM) image of a C_{60} particle in the C_{60}/Cu_2SnSe_3 composite.

3.2. Electrical Transport Properties

Figure 7 shows the temperature dependence of electrical conductivity (σ) for C_{60}/Cu_2SnSe_3 composites with different vol % C_{60}. It can be seen that the σ of the Cu_2SnSe_3 matrix decreases approximately linearly with rising temperature over the measured temperature range, indicating a typical behavior of a heavily-doped semiconductor. The similar tendency of σ was also observed in C_{60}/Cu_2SnSe_3 composites. In addition, the σ of C_{60}/Cu_2SnSe_3 composites decreases with increasing C_{60} content, which should be attributed to the enhanced carrier scattering at the incoherent interfaces between well-dispersed C_{60} clusters and the Cu_2SnSe_3 matrix. Generally, in the case of carriers primarily scattered by grain barriers or interfaces between the second phase and matrix in the composites, the carrier mobility can be written as [22]

$$\mu_H = \frac{eb}{\sqrt{8k_BTm^*}} e^{-\frac{E_B}{k_BT}} \quad (1)$$

where b is the average grain size, k_B the Boltzmann constant, m^* the carrier effective mass, and E_B the activation energy characterizing the barrier height between the matrix and the second phase. As the relative density of the xC_{60}/Cu_2SnSe_3 composite is higher than 97%, the porosity effect can be eliminated. Table 1 lists some physical and structural parameters of xC_{60}/Cu_2SnSe_3 composites at room temperature. As the C_{60} could act as an electron acceptor in the p-type C_{60}/Cu_2SnSe_3 composite, the carrier concentration increases with increasing C_{60} content, which is consistent with the results of Blank [15]. In addition, it can be noted that the carrier mobility decreases with increasing C_{60} content. Therefore, the σ of xC_{60}/Cu_2SnSe_3 composites decreases compared with the σ of the Cu_2SnSe_3 matrix.

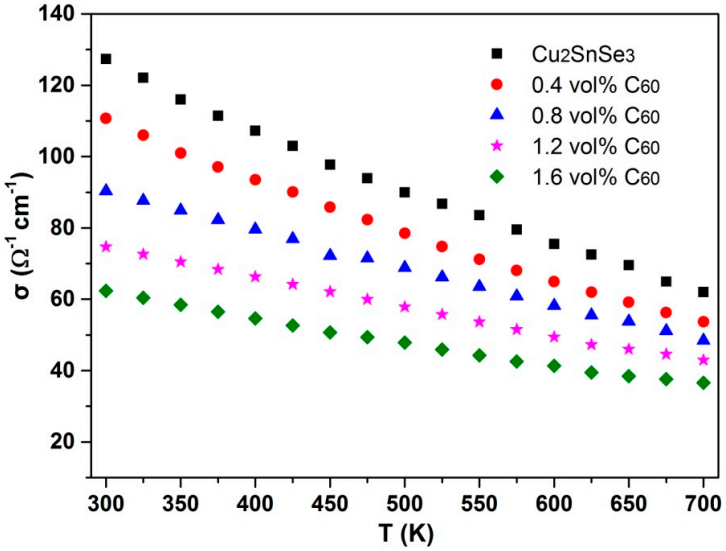

Figure 7. Temperature dependence of electrical conductivity (σ) of C_{60}/Cu_2SnSe_3 composites.

Table 1. Chemical composition, some physical and structural parameters of xC_{60}/Cu_2SnSe_3 composites at room temperature.

x (vol %)	Relative Density	σ ($\Omega^{-1}\cdot cm^{-1}$)	p ($10^{19}cm^{-3}$)	μ_H (cm^2/Vs)	α (μV/K)	κ_L ($Wm^{-1}\cdot K^{-1}$)	m^* (m_0)
0	98.7%	127	3.74	21.2	131	2.77	2.6
0.4	97.2%	110	4.81	14.3	165	2.22	2.8
0.8	98.9%	90	5.01	11.2	188	2.06	2.9
1.2	98.2%	75	4.98	9.4	225	1.96	3.1
1.6	97.9%	62	5.09	7.6	252	1.81	3.2

Figure 8 displays the Seebeck coefficient (α) of xC$_{60}$/Cu$_2$SnSe$_3$ composites as a function of temperature. All composites have a positive α across the whole temperature range, indicating that the holes are major carriers. With rising temperature, the α of all xC$_{60}$/Cu$_2$SnSe$_3$ composites increases approximately linearly and the α of 1.6% C$_{60}$/Cu$_2$SnSe$_3$ composite reaches 314 μV/K at 700 K. Moreover, the α of xC$_{60}$/Cu$_2$SnSe$_3$ composites significantly increases with the increasing content of C$_{60}$. At room temperature, the α increases from 130 μV/K for the Cu$_2$SnSe$_3$ matrix to 252 μV/K for the 1.6 vol % C$_{60}$/Cu$_2$SnSe$_3$ composite. The enhancement of α of xC$_{60}$/Cu$_2$SnSe$_3$ composites should be related to the "energy filter" effect. The Seebeck coefficient can be expressed as [23],

$$\alpha = -\frac{\pi}{3}\frac{k_B}{e}k_B T\frac{d\ln\sigma(E)}{dE}|_{E=E_F} - \frac{T}{n(E)}\frac{dn(E)}{dE}|_{E=E_F} \quad (2)$$

where k_B, σ(E), and n(E) are Boltzmann constant, electrical conductivity, and value of density of states (DOS), respectively. Many studies have confirmed that when nano-phases or nano-inclusions are incorporated into a semiconducting matrix material, the band bending at the inclusion/matrix interface will produce a potential energy barrier which could effectively block low energy electrons, while transmitting high energy electrons [24]. This "electron energy filter" could evidently increase the local density of states near the Fermi level (E_F) and enhance the Seebeck coefficient.

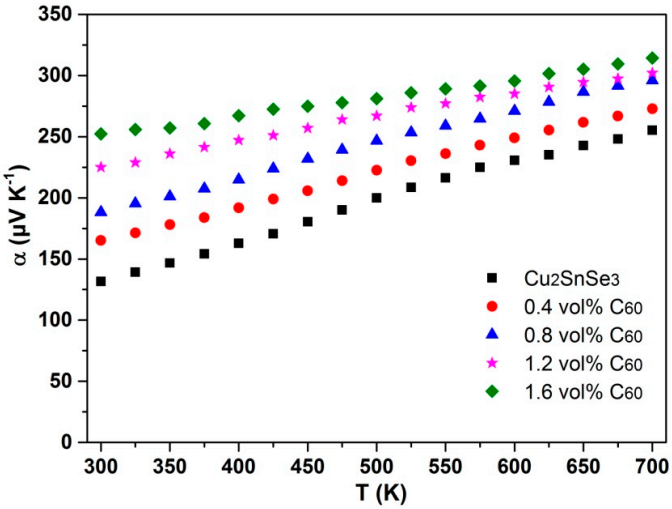

Figure 8. Temperature dependence of Seebeck coefficient (α) of C$_{60}$/Cu$_2$SnSe$_3$ composites.

The μ$_H$ of xC$_{60}$/Cu$_2$SnSe$_3$ composites is shown in Figure 9. The μ_H of xC$_{60}$/Cu$_2$SnSe$_3$ composites decreases with increasing C$_{60}$ content. In addition, the μ$_H$ of xC$_{60}$/Cu$_2$SnSe$_3$ composites was in the order of 10 cm$^2\cdot$V$^{-1}\cdot$s^{-1} at room temperature, which was close to that of skutterudites [25,26]. It may be caused by the similar carrier effective mass of Cu$_2$SnSe$_3$ and CoSb$_3$ compounds. The m* can be estimated in the single parabolic band model using the following equations,

$$m^* = \frac{h^2}{2k_B T}\left(\frac{n}{4\pi F_{\frac{1}{2}}(\eta)}\right)^{2/3} \quad (3)$$

$$\alpha = -\frac{k_B}{e}\left[\frac{(r+2)F_{r+1}(\eta)}{(r+1)F_r(\eta)} - \eta\right] \quad (4)$$

where F_r, h, and r are Fermi integral, Planck's constant, and scattering parameter of relaxation time, respectively. The evaluated equivalent carrier effective mass of xC$_{60}$/Cu$_2$SnSe$_3$ composites at room temperature is listed in Table 1. It can also be seen from Figure 9 that the μ$_H$ of pure Cu$_2$SnSe$_3$ shows a temperature dependence of $T^{-1.5}$ above 500 K, indicating that the acoustic phonon scattering is

dominant in the temperature range from 500 to 700 K. Below 500 K, the μ_H of pure Cu_2SnSe_3 has a weak temperature dependence relationship and the relationship of $\mu_H \propto T^{-0.5}$ is observed, suggesting that a dominative mechanism is alloy scattering. However, the μ_H of xC_{60}/Cu_2SnSe_3 composites deviates from the $T^{-1.5}$ or $T^{-0.5}$ dependence over the entire temperature range, indicating that a mixed scattering mechanism dominates these samples.

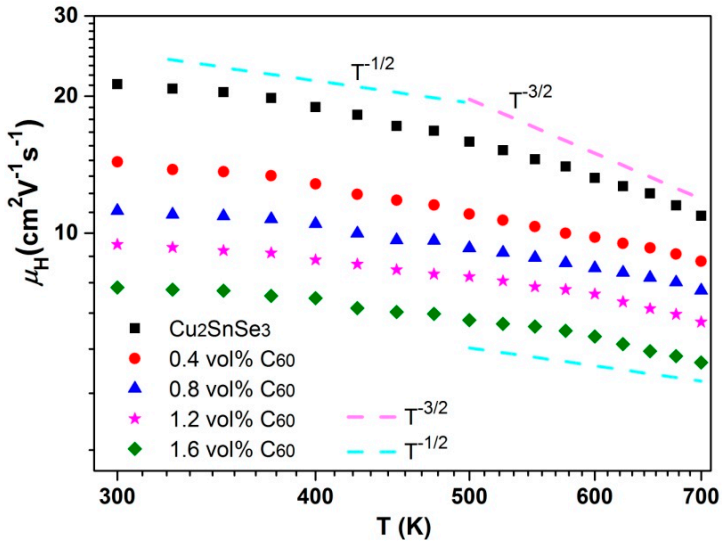

Figure 9. Temperature dependence of carrier mobility (μ_H) of C_{60}/Cu_2SnSe_3 composites.

3.3. Thermal Transport Properties

Figure 10 displays the temperature dependence of total thermal conductivity (κ) and lattice thermal conductivity (κ_L) for C_{60}/Cu_2SnSe_3 composites. The κ_L is estimated by subtracting the electronic contribution via the Wiedmann–Franz law ($\kappa_E = L_0 \sigma T$, where the Lorenz number L_0 is taken as a constant of 2.0×10^{-8} V^2/K^2) from the total thermal conductivity. The κ for all samples declines with increasing temperature. Moreover, the κ of xC_{60}/Cu_2SnSe_3 composites decreases with increasing C_{60} content. The achieved κ of 1.6 vol % C_{60}/Cu_2SnSe_3 composite at room temperature is 1.85 W/mK, which is 34% lower than that of pure Cu_2SnSe_3. The minimal κ of 1.6 vol % C_{60}/Cu_2SnSe_3 composite is 0.71 W/mK at 700 K. It is well-known that the grain boundary, wide or point defects, porosity, and impurity could contribute to the decrease of κ. Owing to high relative density of C_{60}/Cu_2SnSe_3 composites, the reduction of κ originating from the porosity is negligible. Meanwhile, the calculation of κ_E shows that the reduction of κ_E has a limited contribution to the decrease of κ. Therefore, the decrease of κ for C_{60}/Cu_2SnSe_3 composites mainly originates from the depression of κ_L due to the enhancement of phonon scattering by the C_{60} inclusions or nano-particles in the composite. Just as shown in Figure 10b, the κ_L of C_{60}/Cu_2SnSe_3 composites drastically decreases with the content of C_{60} increasing. The minimal κ_L achieved in the present work is 0.68 W/mK at 700 K for the 1.6 vol % C_{60}/Cu_2SnSe_3 sample, which is 43% lower than that of pure Cu_2SnSe_3. According to the kinetic theory [27], the minimum lattice thermal conductivity κ_{Lmin} can be obtained when the phonon mean free path reaches the shortest interatomic distance. The κ_{Lmin} can be estimated from the formula $\kappa_L = 1/3 C_v \nu_m l$, where C_v is heat capacity per unit volume of the system using Dulong and Petit value, ν_m the mean sound velocity, and l the mean free path of phonon. The ν_m comes from the data in reference [28]. If we assume the minimum l to be the interatomic distance for Cu_2SnSe_3 (0.238 nm), the κ_{Lmin} is calculated as 0.52 $Wm^{-1} \cdot K^{-1}$, just as shown by dashed line in Figure 10b. The κ_L of 1.6 vol % C_{60}/Cu_2SnSe_3 composites approaches the κ_{Lmin} of Cu_2SnSe_3 at high temperature.

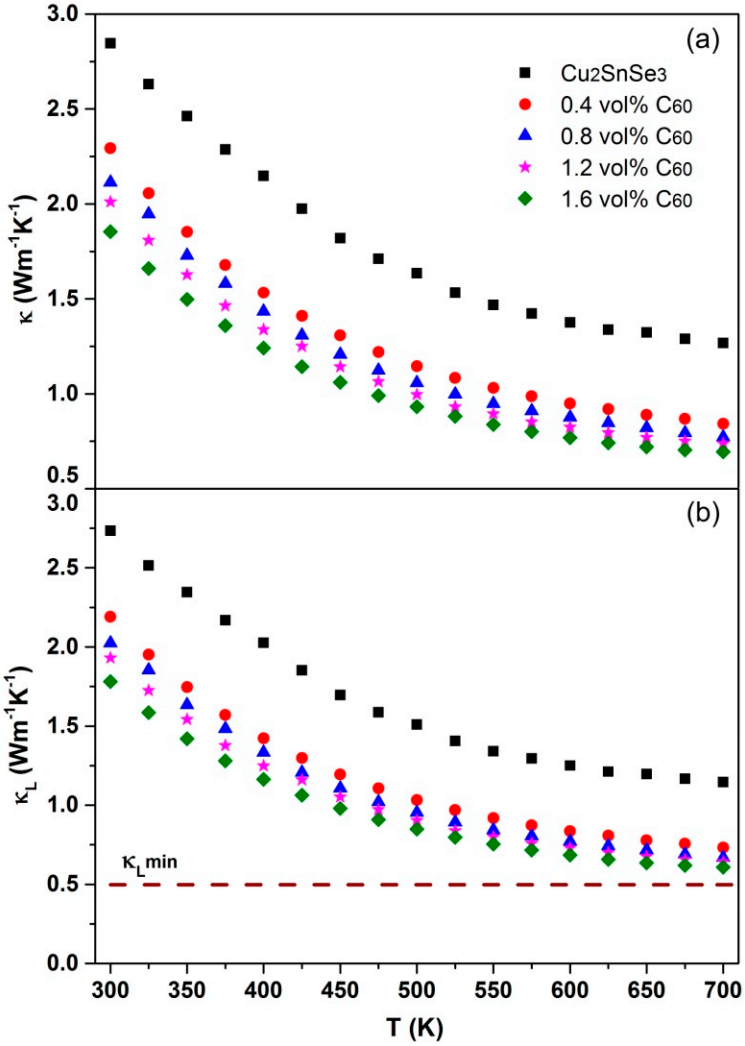

Figure 10. (**a**) Temperature dependence of total thermal conductivity (κ) of C_{60}/Cu_2SnSe_3 composites; (**b**) temperature dependence of lattice thermal conductivity (κ_L) of C_{60}/Cu_2SnSe_3 composites.

3.4. Figure of Merit

The conversion efficiency of TE materials depends on the maximum dimensionless figure of merit (ZT). Figure 11 shows the dimensionless figure of merit (ZT) of C_{60}/Cu_2SnSe_3 composites as a function of temperature. Like other doped Cu_2SnSe_3 investigated before [8,29,30], the ZT value of C_{60}/Cu_2SnSe_3 composites increases approximately linearly with increasing temperature. Compared with the ZT of the Cu_2SnSe_3 sample, the ZT value of C_{60}/Cu_2SnSe_3 composites is enhanced. For the 0.8 vol % C_{60}/Cu_2SnSe_3sample, the maximum ZT value is 0.38 at 700 K, which is 45% higher than that of the pure Cu_2SnSe_3 sample. The enhancement of ZT for C_{60}/Cu_2SnSe_3 composites is mainly attributed to the reduced κ_L and the enhanced α. The addition of C_{60} into the Cu_2SnSe_3 matrix could improve the TE properties, which is a promising process to the design Cu-based chalcogenide compounds with high TE performance. When the material with optimized carrier concentration is selected as the matrix, the higher ZT value of TE composite could be achieved.

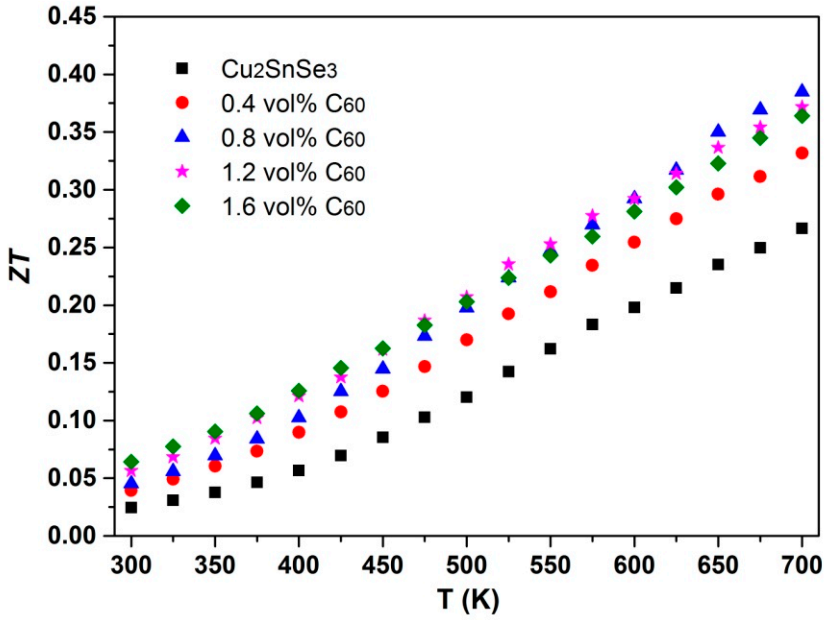

Figure 11. Temperature dependence of the dimensionless figure of merit of (*ZT*) of C_{60}/Cu_2SnSe_3 composites.

4. Conclusions

In this study, C_{60} was incorporated into a Cu_2SnSe_3 matrix, and C_{60}/Cu_2SnSe_3 composites were fabricated using BM-SPS method. The C_{60} phase distributed uniformly in the form of clusters, and the average cluster size was less than 1 μm. With increasing C_{60} content, the electrical conductivity of C_{60}/Cu_2SnSe_3 composites decreased, while the Seebeck coefficient of C_{60}/Cu_2SnSe_3 composites increased due to the "electron energy filter" of the C_{60} nano-phase. The thermal conductivity of C_{60}/Cu_2SnSe_3 composites decreased significantly, which originated from the phonon scattering by the C_{60} clusters located on the grain boundaries of the Cu_2SnSe_3 matrix. The maximum *ZT* of 0.38 was obtained at 700 K for 0.8 vol % C_{60}/Cu_2SnSe_3 composite.

Acknowledgments: This work was supported in part by National Natural Science Foundations of China (51202088 and 51271087) and the Opening Project of State Key Laboratory of High Performance Ceramics and Superfine Microstructure (SKL201405SIC).

Author Contributions: The manuscript was completed through contributions of all authors. Degang Zhao and Jiai Ning performed the experiments. Degang Zhao wrote the paper. Jiai Ning and Min Zuo contributed to the data analysis.

Conflicts of Interest: The authors declare no conflicts of interest.

References

1. Disalvo, F.J. Thermoelectric cooling and power generation. *Science* **1999**, *285*, 703–706. [CrossRef] [PubMed]
2. Yu, Y.; Lv, L.; Wang, X.Y.; Zhu, B.; Huang, Z.; Zu, F.Q. Influence of melt overheating treatment on solidification behavior of Bi_2Te_3-based alloys at different cooling rates. *Mater. Des.* **2015**, *88*, 743–750.
3. Liu, W.S.; Yan, X.; Chen, G.; Ren, Z.F. Recent advances in thermoelectric nanocomposites. *Nano Energy* **2012**, *1*, 42–56. [CrossRef]
4. Wan, S.; Huang, X.Y.; Qiu, P.F.; Bai, S.Q.; Chen, L.D. The effect of short carbon fibers on the thermoelectric and mechanical properties of p-type $CeFe_4Sb_{12}$ skutterudite composites. *Mater. Des.* **2015**, *67*, 379–384. [CrossRef]
5. Zerer, W.G.; Lalonde, A.; Gibbs, Z.M.; Heinrich, C.P.; Panthofer, M.; Snyder, G.J.; Tremel, W. Influence of a nano phase segregation on the thermoelectric properties of the p-type doped stannite compound $Cu_{2+x}Zn_{1-x}GeSe_4$. *J. Am. Chem. Soc.* **2012**, *134*, 7147–7154. [CrossRef] [PubMed]

6. Raju, C.; Falmbigl, M.; Rogl, P.; Heinrich, P.; Royanian, E.; Bauer, E.; Mallik, R.C. Thermoelectric properties of Zn doped Cu_2SnSe_3. *Mater. Chem. Phys.* **2014**, *147*, 1022–1028. [CrossRef]
7. Liu, G.H.; Li, J.T.; Chen, K.X.; Li, Y.; Zhou, M.; Han, Y.M.; Li, L.F. Direct fabrication of highly-dense $Cu_2ZnSnSe_4$ bulk materials by combustion synthesis for enhanced thermoelectric properties. *Mater. Des.* **2016**, *93*, 238–246. [CrossRef]
8. Shi, X.Y.; Xi, L.L.; Fan, J.; Zhang, W.Q.; Chen, L.D. Cu-Se bond network and thermoelectric compounds with complex diamondlike structure. *Chem. Mater.* **2010**, *22*, 6029–6031. [CrossRef]
9. Fan, J.; Liu, H.L.; Shi, X.Y.; Bai, S.Q.; Shi, X.; Chen, L.D. Investigation of thermoelectric properties of $Cu_2Ga_xSn_{1-x}Se_3$ diamond-like compounds by hot pressing and spark plasma sintering. *Acta Mater.* **2013**, *61*, 4297–4304. [CrossRef]
10. Skoug, E.J.; Cain, J.D.; Morelli, D.T. Thermoelectric properties of the Cu_2SnSe_3-Cu_2GeSe_3 solid solution. *J. Alloy. Compd.* **2012**, *506*, 18–23. [CrossRef]
11. Lan, Y.C.; Minnich, A.J.; Chen, G.; Ren, Z.F. Enhancement of thermoelectric figure of merit by a bulk nanostructuring approach. *Adv. Funct. Mater.* **2010**, *20*, 357–376. [CrossRef]
12. Zolriasatein, A.; Yan, X.; Bauer, E.; Rogl, P. Influence of PCA on thermoelectric properties and hardness of nanostructured Ba-Cu-Si clatherates. *Mater. Des.* **2015**, *87*, 883–890.
13. Zebarjadi, M.; Esfarjani, K.; Ren, Z.F.; Chen, G. Perspectives on thermoelectric: From fundamentals to device applications. *Energy Environ. Sci.* **2012**, *5*, 5147–5162. [CrossRef]
14. Kim, K.T.; Choi, S.Y.; Shin, E.H.; Moon, K.S.; Ha, G.H. The influence of CNTs on the thermoelectric properties of a CNT/Bi_2Te_3 composite. *Carbon* **2013**, *52*, 541–549. [CrossRef]
15. Blank, V.D.; Buga, S.G.; Kulbachinskii, V.A.; Kytin, V.G.; Stepanov, P.B. Thermoelectric properties of $Bi_{0.5}Sb_{1.5}Te_3/C_{60}$ nanocomposites. *Phys. Rev.* **2012**, *86*, 64–70. [CrossRef]
16. Kulbachinskii, V.A.; Kytin, V.G.; Popov, M.Yu.; Buga, S.G.; Blank, V.D. Composites of $Bi_{2-x}Sb_xTe_3$ nanocrystals and fullerene molecules. *J. Solid State Chem.* **2012**, *193*, 64–70. [CrossRef]
17. Shi, X.; Chen, L.; Yang, J.; Meisner, G.P. Enhanced thermoelectric figure of merit of $CoSb_3$ via large-defect scattering. *Appl. Phys. Lett.* **2004**, *84*, 2301–2303. [CrossRef]
18. Itoh, T.; Ishikawa, K. Effects of fullerene addition on thermoelectric properties of *n*-type skutterudite compound. *J. Mater. Res.* **2007**, *22*, 249–255. [CrossRef]
19. Nandihlli, N.; Lahwal, A.; Holgate, T.C.; Tritt, T.M. Thermoelectric properties of composites made of $Ni_{0.05}Mo_3Sb_{5.4}Te_{1.6}$ and fullerene. *J. Solid State Chem.* **2013**, *203*, 25–30. [CrossRef]
20. Faleev, S.V.; Leonard, F. Theory of enhancement of thermoelectric properties of materials with nanoinclusions. *Phys. Rev.* **2008**, *77*, 214304. [CrossRef]
21. Zebarjadi, M.; Esfarjani, K.; Shakouri, A.; Zeng, G.; Lu, H.; Zide, J.; Gossard, A. Effect of nanoparticle scattering on thermoelectric power factor. *Appl. Phys. Lett.* **2009**, *94*, 202105. [CrossRef]
22. Orton, J.W.; Powell, M.J. The Hall effect in polycrystalline and powdered semiconductors. *Rep. Prog. Phys.* **1980**, *43*, 1263–1307. [CrossRef]
23. Zhao, D.G.; Zuo, M.; Geng, H.R. Synthesis and thermoelectric properties of $CoSb_3/WO_3$ thermoelectric composites. *Intermetallics* **2013**, *40*, 71–75. [CrossRef]
24. Xiong, Z.; Chen, X.H.; Huang, X.Y.; Bai, S.Q.; Chen, L.D. High thermoelectric performance of $Yb_{0.26}Co_4Sb_{12}/y$GaSb nanocomposites originating from scattering electrons of low energy. *Acta Mater.* **2010**, *58*, 3995–4002. [CrossRef]
25. Xi, L.L.; Yang, J.; Lu, C.F.; Chen, L.; Zhang, W.Q. Systematic study of the multiple-element filling in caged skutterudite $CoSb_3$. *Chem. Mater.* **2010**, *22*, 2384–2394. [CrossRef]
26. Shi, X.; Yang, J.; Salvador, J.R.; James, R. Multiple-filled skutterudites: High thermoelectric figure of merit through separately optimizing electrical and thermal transports. *J. Am. Chem. Soc.* **2011**, *133*, 7837–7846. [CrossRef] [PubMed]
27. Morelli, D.T.; Jovovic, V.; Heremans, J.P. Intrinsically minimal thermal conductivity in cubic I-V-VI_2 semiconductors. *Phys. Rev. Lett.* **2008**, *101*, 035901. [CrossRef] [PubMed]
28. Cho, J.Y.; Shi, X.; Salvador, J.R.; Meisner, G.P. Thermoelectric properties and investigations of low thermal conductivity in Ga-doped Cu_2GeSe_3. *Phys. Rev.* **2011**, *84*, 085207. [CrossRef]

29. Liu, F.S.; Wang, B.; Ao, W.Q.; Li, Y.; Li, J.Q. Crystal structure and thermoelectric properties of $Cu_2Cd_{1-x}Zn_xSe_4$ solid solutions. *Intermetallics* **2014**, *55*, 15–21. [CrossRef]
30. Do, D.T.; Mahanti, S.D. Theoretical study of defects Cu_3SbSe_4: Search for optimum dopants for enhancing thermoelectric properties. *J. Alloy. Compd.* **2015**, *625*, 346–354. [CrossRef]